Postprint of: Pierpaoli M., Jakobczyk P., Sawczak M., Łuczkiewicz A., Fudala-Książek S., Bogdanowicz R., Carbon nanoarchitectures as high-performance electrodes for the electrochemical oxidation of landfill leachate, Journal of Hazardous Materials, Vol. 401 (2021), 123407, DOI: 10.1016/j.jhazmat.2020.123407

Carbon nanoarchitectures as high-performance electrodes for the electrochemical oxidation of landfill leachate

Mattia Pierpaoli[a], Paweł Jakobczyk[a], Mirosław Sawczak[b],
Aneta Łuczkiewicz[c], Sylwia Fudala-Książek[c], Robert Bogdanowicz[a]

[a] *Faculty of Electronics, Telecommunications And Informatics,*
Gdańsk University of Technology, ul. G. Narutowicza 11/12, 80-233 Gdańsk (Poland);

[b] *The Szewalski Institute of Fluid-Flow Machinery, Polish Academy of Sciences,*
Generała Józefa Fiszera 14, 80-231 Gdańsk (Poland);

[c] *Faculty of Civil and Environmental Engineering,*
Gdańsk University of Technology, ul. G. Narutowicza 11/12, 80-233 Gdańsk (Poland).

Corresponding author:

Mattia Pierpaoli, PhD.

mattia.pierpaoli@pg.edu.pl

Faculty of Electronics, Telecommunications and Informatics

Gdańsk University of Technology,

Gabriela Narutowicza 11/12,

80-980 Gdańsk (Poland)

Carbon nanoarchitectures as high-performance electrodes for the electrochemical oxidation of landfill leachate

Mattia Pierpaoli[a], Paweł Jakobczyk[a], Mirosław Sawczak[b],
Aneta Łuczkiewicz[c], Sylwia Fudala-Książek[c], Robert Bogdanowicz[a]

[a] *Faculty of Electronics,Telecommunications And Informatics, Gdansk University of Technology, Poland*

[b] *Polish Academy of Sciences, The Szewalski Institute of Fluid-Flow Machinery, Poland*

[c] *Faculty of Civil and Environmental Engineering, Gdansk University of Technology, Poland*

Abstract

Nanomaterials and assemblies of the aforementioned into complex architectures constitute an opportunity to design efficient and selective solutions to widespread and emerging environmental issues. The limited disposal of organic matter in modern landfills generates extremely concentrated leachates characterised by high concentrations of refractory compounds. Conventional biochemical treatment methods are unsuitable, while advanced treatment, such coagulation, reverse osmosis and ultrafiltration can be very costly and generate additional waste. Electrochemical oxidation is an established technique to efficiently mineralise a plethora of recalcitrant pollutants, however the selectivity and efficiency of the process are strongly related to the anode material. For this reason, a nanoarchitectured carbon material has been designed and synthesised to improve the capability of the anode towards the adsorption and decomposition of pollutants. Instead of simple nanostructures, intelligently engineered nanomaterials can come in handy for more efficient advanced treatment techniques. In this study, a carbon nanoarchitecture comprising boron-doped vertically aligned graphene walls (BCNWs) were grown on a boron-doped diamond (BDD) interfacial layer. The results show how the peculiar maze-like morphology and the concurrence of different carbon hybridisations resulted in a higher current exchange density. The BDD performed better for the removal of NH_4^+ while the BCNW-only sample exhibited a faster deactivation. The BDD/BCNW nanoarchitecture resulted in an enhanced COD removal and a NH_4^+ removal similar to that of BDD, without the intermediate production of NO_2^- and NO_3^-.

Keywords

advanced oxidation, vertical graphene, carbon nanowalls, refractory pollutant, boron-doped diamond

1. Introduction

Historical and current patterns of natural resource use have led to environmental degradation and put human health at risk. With the introduction of the 1999/31/EC Directive (European Parliament, 1999) and the 2013/39/EU Directive (European Parliament, 2013), a new waste hierarchy has been introduced, jointly with a list of 45 new pollutants of emerging interest. This has drawn attention to landfill leachates (LLs), which are significant sources of macro- and micropollutants (Fudala-Ksiazek et al., 2017, 2016), and are characterised by low biodegradability. Thus, conventional biochemical methods are unsuitable for the treatment of LLs, while other processes such as chemical oxidation, coagulation, reverse osmosis and ultrafiltration can be very costly. For this reason, the EU is supporting the development of innovative wastewater treatment technologies to enable cheaper and more sustainable treatment (European Parliament, 2013).

Electrochemical oxidation (EO) of water pollutants is an advanced oxidation process (AOP), which mineralises organic and inorganic pollutants. Among other AOPs, EO benefits from the lack of added chemicals as well as the lack of the necessity to dispose of secondary waste products. The main requirement for the electrodes is that they need to possess a wide electrochemical window, to ensure stability for extended usage. For this reason, the electrode material plays a primary role in the EO process (Pierpaoli et al., 2020b). Iridium, platinum, ruthenium and titanium oxide-based anodes are characterised by high electrocatalytic activity, leading to faster degradation of organics at lower potentials, while lead, tin oxides and boron-doped diamond (BDD) electrodes support the complete mineralisation of organics due to their high oxygen evolution overpotential. Because of the inexpensiveness and easy availability of graphite, graphitic electrodes have been tested by a few authors for their potential at oxidising organic matter and ammonia from LLs (Bashir et al., 2009; Chiang et al., 1995) However, the likelihood of the limited working potential range being exceeded due to working conditions would lead to a significant dissolution of the graphite electrode (Qiao et al., 2018). Dimensionally Stable Anodes (DSAs) form a class of electrodes including several kinds of metal oxides (such as RuO_2, IrO_2, SnO_2) coated on titanium substrates. Given their ease of preparation by the hydrothermal method, and their wider working potential, many authors have investigated the removal efficiency of such electrodes. In particular, a few metal oxides in DSAs are known to promote the formation of chloride radicals with respect to the water oxidation. The thus-produced chlorine, hypochlorite, and hypochlorous acid play an important role in the indirect pollutant oxidation; however, many organochlorinated species may be present as intermediate by-products, which can constitute a hazard more harmful than the original pollutants (Sirés et al., 2014).

Simultaneously to the investigation of the removal of new emerging pollutants using conventional electrodes, the scientific community shift its attention to the realisation of novel nanostructured electrode materials, as they exhibit better electrochemical properties than their bulk

counterparts (Pierpaoli et al., 2020a). Compared to naturally occurring porous materials with a pre-determined pore dimension distribution, nanostructured hierarchical porous materials with well-defined pore morphology offer a maximised surface area and a minimised diffusive resistance to mass transport (Dutta et al., 2014). For this reason, the development of highly sophisticated assemblies of nanomaterials may lead to further performance refinements(Kaneti et al., 2017; Malgras et al., 2015; Wang et al., 2018), making them suitable for real-world application.

While a plethora of structured nanomaterials have been developed for environmental photocatalysis, the enhanced selective adsorption of various pollutants and other functional applications (Dutta et al., 2017), few examples in which they have been used for other remediation techniques are reported in the literature. In particular, while nanostructured electrodes have been widely used for sensing applications, a limited number of studies report their use for environmental remediation. Tan and coauthors prepared a nanoporous PbO_2 electrode, firstly by synthesising highly-ordered TiO_2 nanotubes, then by depositing PbO_2 by the pulse electrodeposition method (Tan et al., 2011). Because of the porous microstructure, in which the diffusion of the electrolyte is locally restricted, the pH is much lower than in the bulk electrolyte. Similarly, Wang et al. prepared different nanotube-based architectures by tailoring the electrode production conditions. By varying the anodisation time and voltage, both morphological and electrochemical properties varied, resulting in an 85 nm pore diameter, which is optimum for catalytic performance (Wang et al., 2013). The higher electrochemical efficiency was correlated with a higher oxygen evolution potential. In another study, Zhang and coworkers synthesised a Ti/SnO_2-Sb electrode, modified by carbon nanotubes to indirectly increase the specific surface area and the number of reaction active sites (Zhang et al., 2014). In this work, carbon nanotubes played the role of a template, which was burned off during calcination. When carbon-based electrodes are investigated, BDD is favoured because of its high chemical inertness, corrosion resistance, and widest working potential, while graphite constitutes a cost-effective solution. In BDD synthesis, the sp^3/sp^2 carbon hybridisation ratio has been found to be an important parameter, linked to promoting the active or non-active electrode behaviour (Medeiros De Araújo et al., 2014) and the boron inclusion into the diamond lattice (Bogdanowicz et al., 2013), resulting in different EO selectivity (Fudala-Ksiazek et al., 2018). Boron-doped carbon nanowalls (BCNWs) are open boundaries - vertically oriented few-layer graphene sheets - possessing extraordinary electrochemical properties. Because of their peculiar maze-like morphology, the specific surface area is increased, compared to a BDD electrode, which suggests an enhanced efficiency towards the degradation of various pollutants, with a potential window comparable to BDDs (Hiramatsu and Hori, 2010; Sobaszek et al., 2017). The vertical alignment of the carbon nanostructures affects the electrochemical performance in different ways, both due to the chemistry and to the morphology of the CVD-growth architecture. The larger extends of exposed edges, compared to a parallel alignment, allows to have a greater number of functional groups and

chemisorbed heteroatoms, in particular oxygen, which allows a higher reactivity of the carbonaceous nanostructure (Dettlaff et al., 2020). Many physical properties of the synthesized carbon nanomaterials, in particular the wetting and adsorption behaviour, are decisively influenced by chemisorbed oxygen. Oxygen, in the plane edges, can be bound in the form of various functional groups, thus they play an important contribution to the capacitance through faradic processes which involve one or two-electron transfer reactions, which aspect is limited in the case of a parallel disposition of the carbon layers.

In this study, for the first time, a hybrid 3D/2D carbon nanoarchitectured electrode was fabricated, and the oxidation efficiency was assessed by the electrochemical mineralisation of recalcitrant landfill leachate pollutants. The three-dimensional layer consisted of a BDD sheet grown by microwave plasma-enhanced chemical vapour deposition (MPECVD) on a roughened niobium substrate. By changing the composition of the gas during the synthesis process, it was possible to grow vertically aligned graphene sheets on the uneven surface of the substrate, with a BDD interlayer, covered by “nano-flap” surface nanotextures. BDD and graphite electrodes were used as a reference for comparison.

2. Materials and methods

2.1 Landfill leachate analysis

In this study, LL was collected from a waste cell at a municipal solid waste plant (MSWP) located in northern Poland (N 54°51′742′ S 18°36′854″) which serves a metropolitan area of approximately 460,000 people and receives approximately 200,000 Mg of waste annually. The landfill was operated from January 2003 to November 2011. During that time, the cells were arranged in an ad-hoc manner without any liner or pollution-control systems, and with unlimited disposal of organic wastes. While in operation, the landfill received up to 90% of indistinct municipal waste, including the deposition of highly biodegradable waste. The LL was collected in March 2019, after 195 months (16 years and 3 months) of operation. This explains the high COD (2854 mg O_2/l), and low BOD_5 (mg O_2/l) and BOD_{20} (345 mg O_2/l) concentrations. The LL was also characterised by a high ammonia concentration (1940 mg N-NH_4^+/l), which constituted the main fraction of the total nitrogen (98% of TN). Ammonia forms in a landfill cell during the decomposition of organic matter (mainly proteins) and, as a water-soluble compound, is easily released into the leachate, because its microbiological utilisation is limited under low oxygen availability. Phosphorus was also detected, mainly in mineral form, as P-PO_4^{3-}mg/l and constituted about 89% of the total phosphorous (TP). The presence of phosphorus and nitrogen mainly in mineral form as well as the low BOD_5/COD (0.08) and BOD_5/BOD_{20} (0.63) ratios indicated that the biodegradable organic matter from the solid waste was efficiently consumed. In manure landfills, the organic matter becomes refractory and is mainly represented by humic and fulvic-like fractions

(Pelaez et al., 2009), which can be indirectly confirmed by the leachate colour. It is worth highlighting that the WC/PP generates landfill gas which is stable in quantity (44,881 m^3 in March) and quality (about 73% methane), suggesting that this cell still undergoes a methanogenic phase (Spagni et al., 2008). The leachate characteristics are reported in Table 1.

Table 1 – Leachate characteristics

Parameter	Value
pH	7.78
Redox potential (mV)	-409.7
BOD_5 (mg O_2/l)	218
BOD_{20} (mg O_2/l)	345
COD (mg O_2/l)	2854
$N\text{-}NH_4^+$ (mg/l)	1940
S^{2-} (mg/l)	10.5
Cl^- (mg/l)	2758
SO_4^- (mg/l)	1035
TN (mg/l)	1975
$N\text{-}NO_3^-$ (mg/l)	15.2
$N\text{-}NO_2^-$ (mg/l)	0.229
$P\text{-}PO_4^{3-}$ (mg/l)	12.98
TP (mg/l)	14.6

2.2 Nanoarchitectured electrode fabrication

The carbon nanoarchitectures were fabricated as follows: a 2-inch diameter niobium substrate was sandblasted, washed and rinsed with acetone and 2-propanol in an ultrasonic bath, to roughen the surface. Next, the substrate was sonicated in a water-based nanodiamond-slurry, in order to provide the nucleation sites for the growth of thin diamond film (Sobaszek et al., 2017). BDD and BCNW were grown by MPECVD (SEKI Technotron AX5400S, 2.45 GHz, 1300 W), using a gas mixture of H_2, CH_4, B_2H_6, and N_2 (N_2 was used only for growing the BCNW structure). The chamber pressure was kept at 50 Torr for all of the processes. The gas composition, substrate holder temperature and process duration were varied according to Table 2. As can be seen, the process duration between the BCNW and BDD differs because of the different nanostructure growth rates. While the doped diamond can be deposited directly onto the niobium substrate at 700°C, the growth of vertical carbon on Nb has been found to be facilitated by a higher temperature. In order to minimise the internal thermal stresses, both layers of the nanoarchitectured composite were

grown at the same temperature. The growth duration is substantially reduced for the CNW growth because of the higher CH_4 flow and growth rate. To obtain a hierarchical structure, the growth of the graphene "nano-flap", perpendicular to the principal BCNW, was obtained by deliberately switching off the DC bias. In the absence of an electrical field perpendicular to the niobium substrate, the growth proceeds in multiple directions, thus realising a complex interconnected morphology.

Table 2 – Growth parameters for the nanoarchitectured electrode fabrication

	BDD	**BCNW**	**BDD/BCNW**
Substrate		Nb	
Sample holder temperature (°C)	700	850	850
Growth duration (h)	12	3	3+2
B_2H_6/CH_4	2.5	0.3	0.3
N_2/CH_4	0	0.12	0+0.12

The graphite electrode was used as purchased and consists of a 50*40*3mm 99.99% graphitic plate. The sample was cut and covered with resin to have the same dimension as the exposed surface.

2.2 Nanoarchitectured electrode characterisation

For all of the samples, morphological, chemical, and electrochemical characterisations were performed both prior to and after the EO tests. The nomenclature report "pre" or "post", corresponding to whether the test was performed before or after the EO.

Scanning electron microscopy and energy-dispersive X-ray spectroscopy were performed with a Phenom XL instrument (Thermo Fisher Scientific), using a 10 kV beam accelerating voltage with BSD or EDS detectors working in high vacuum mode.

Raman spectra were recorded in the 100–1740 cm^{-1} range, using a micro Raman spectrometer (InVia Renishaw, UK) equipped with a 514 nm argon-ion laser. For each sample, spectra were acquired in three different spots, and the measured values were averaged, smoothed (using a Savitzky-Golay method: 15 points, second polynomial order), and the baseline (approximated with a cubic polynomial) was subtracted and normalised.

The electrochemical properties of the samples were investigated by cyclic voltammetry (CV), electrochemical impedance spectroscopy (EIS), and linear sweep voltammetry (LSV). For each investigation technique, the working electrode was the considered anode, having a working area of 0.0314 cm^2, the counter electrode was a platinum wire, and the reference electrode was an AgCl-

coated Ag wire. The measurement was carried out in 0.5 M H_2SO_4 as the electrolyte, at a scan rate of 50 mV/s, using a potentiostat-galvanostat (VMP-300, *Bio-Logic*, France) driven by the EC-Lab software.

2.3 Nanoarchitectured electrochemical oxidation test

EO tests were performed in a cylindrical single-cell reactor containing 400 mL of solution. The leachate was diluted 1:1 with deionised water. The anode had a total area of 10.5 cm^2, and was secured in a PEEK sample holder (Figure 1a), while a stainless steel net of approximately 10x7 cm served as the cathode. A constant potential of 12V was applied to the electrodes, and the current was measured during the process. The leachate was stirred and thermostated in a water bath for the whole process. The N-NH_4^+ and COD removal processes can happen both by direct and indirect electrochemical oxidation (Figure 1b). The pH, redox potential, and concentration of selected pollutants were monitored every 2 hours. In particular, the following parameters were analysed according to American Public Health Association guidelines (D. Eaton et al., 2005): pH and redox potential (mV) using a portable multi-parameter meter (HL-HQ40d multi, HACH, Germany); total (TN) and inorganic N compounds (N-NH_4^+, N-NO_3^-, and N-NO_2^-), and chemical oxygen demand (COD), using a XION 500 spectrophotometer (Dr. Lange, GmbH, Germany); 5- and 20-day biochemical oxygen demand (BOD5 and BOD20) using the manometric respirometric BOD OxiTop method.

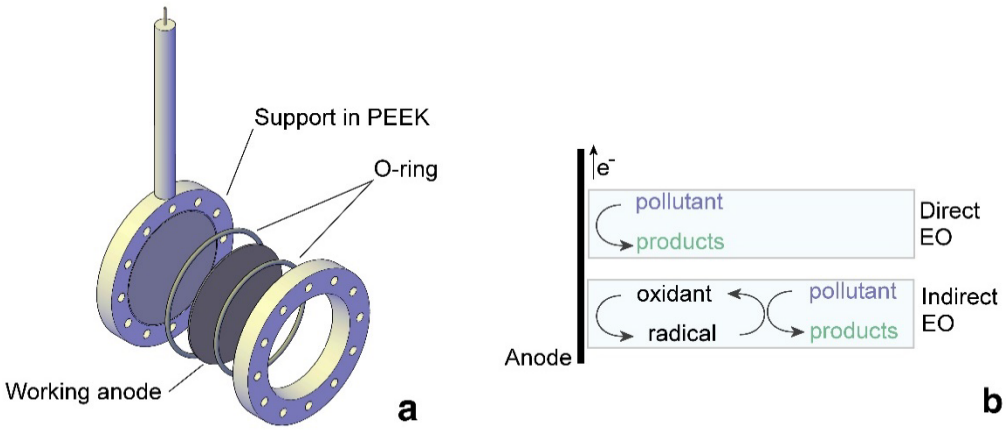

Figure 1 – (a) Sample holder used in the electrochemical oxidation batch test; (b) schematic of the process occurring in the electrochemical oxidation process

3. Results and discussion

3.1 Leachate electrochemical oxidation

The decrease in pollutant concentration during the electrochemical oxidative tests is expressed against the specific electrical charge (Q), as follows:

234 $$Q = \frac{JAt}{V}$$

235 Where J is the current density (Am^{-2}), A is the electrode surface (m^2), t is the time (s), and V is the
236 volume of the electrolytic solution (L). While a representation of the physicochemical parameters
237 against time would determine the oxidation rate, the representation against Q provides information
238 about the process efficiency (Anglada et al., 2009).

239 Figure 2a shows the trend of the COD with Q for the different anode types. After 8 hours of tests, the
240 COD was reduced by about 50% for the BDD electrode; the same result was achieved by the BCNW
241 electrode, but at a lower specific electrical charge (40% lower). The BDD/BCNW sample had the best
242 performance, removing 83% of the COD. The graphite electrode test was performed for only 4 hours
243 because of the accelerated exfoliation of the electrode, and only 12% of the COD was oxidised. BOD_{20}
244 removal was equal to 55% for the BDD electrode, 37% for the BCNW, and it reached 70% for the
245 BDD/BCNW electrode. Interestingly, the ammonium removal was faster with the BDD (Figure 2b),
246 followed by the BCNW and by the nanostructured composite electrode. As ammonia removal is
247 mainly promoted by a reaction with active chlorine, the electrodes which performed better at directly
248 oxidising organic matter resulted in being disadvantaged for the indirect $N\text{-}NH_4^+$ oxidation because
249 of the competitive behaviour. While hypochlorite ions and hypochlorous acid can oxidise ammonium
250 into nitrogen gas due to their high oxidative potentials, BDD has a tendency to oxidise ammonium
251 to nitrates (Figure 2c). The variation of pH for the three nanostructured electrodes (Figure 2d) was
252 small (an increase of 7% after 8 hours), and was constant for the graphite electrode. However, it has
253 to be considered that the pH is significantly lower in the vicinity of the electrode, especially within
254 the pores, due to the CNW maze-like structure, because of the limited electrolyte diffusion (Wang et
255 al., 2013). The presence of chlorine concentration and other oxidants results in an increase of the
256 redox potential. While, for the BDD/BCNW electrode, the oxidation-reduction potential (ORP)
257 increase is higher at 4h, followed by a decrease, this results in an acceleration of the $N\text{-}NH_4^+$ removal.
258 Controversially, the ORP of the BDD sample increases slowly with the time, until a plateau is reached
259 (Figure 2e). Despite the $N\text{-}NH_4^+$ removal being slower with the nanostructured composite, the total
260 nitrogen removal efficiency was similar to the BDD electrode, mostly because of the direct oxidation
261 to nitrogen gas by the chlorine reaction, without the production of nitrates.

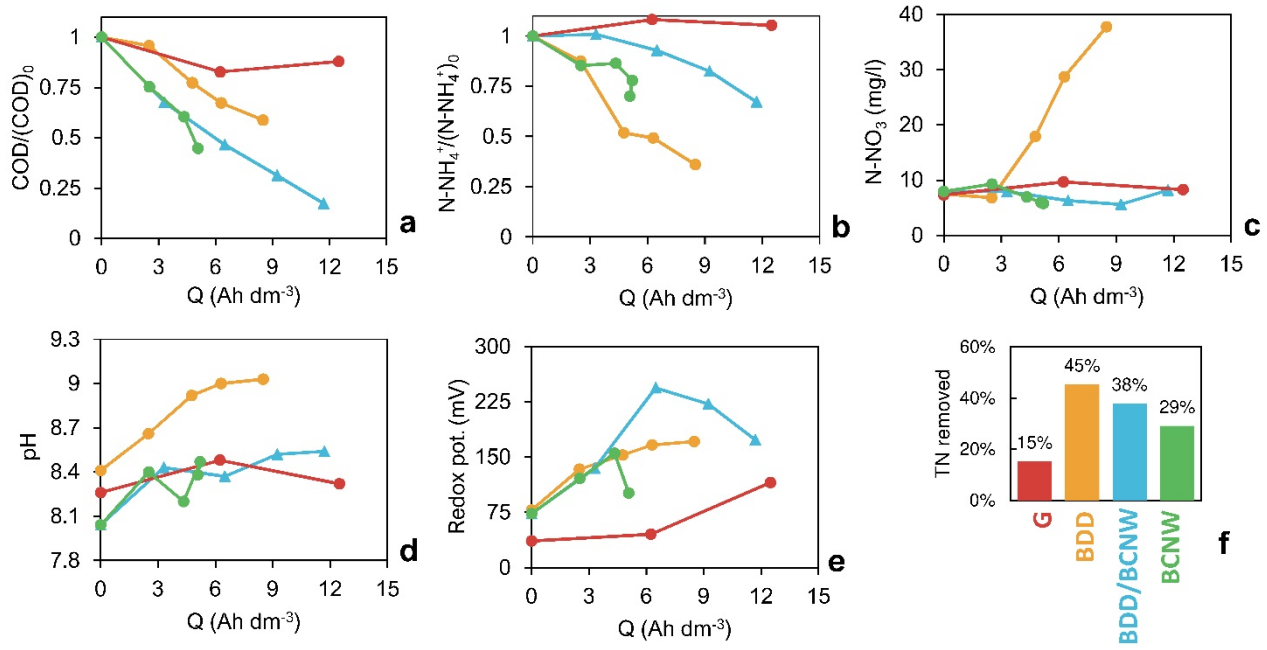

Figure 2 – (a-e) The variation of COD, N-NH_4^+, N-NO_3^-, pH and redox potential with Q for the different consider electrodes; (f) the total nitrogen removed within 8 h (4 h for the graphite electrode) of the test.

3.2 Electrode morphology

The morphology of all of the synthesised samples is affected by the surface pretreatment, resulting from the sandblasting process, which produces microscale valleys having a diameter of tens of micrometers (Figure 3a). Altering the support surface prior to the CVD process is an innovative approach to obtain a carbon nanostructure with concave and convex curvatures in a simple way (Huang et al., 2019).

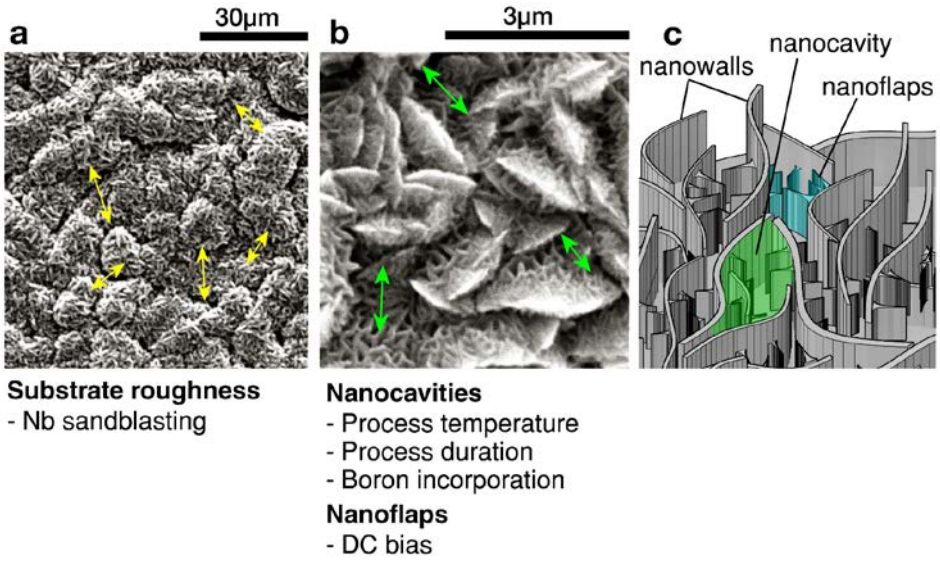

Figure 3 – (a,b) SEM images of the BDD/BCNW grown on Nb. (c) Schematic representation of the BCNW morphology

While this is the only roughness present for the BDD (Figure 4b), where the carbon grows vertically, microcavities, having an opening in the range between tens and hundreds of nanometres, are formed between the nanowall boundaries (Figure 3b). It is easy to tune these openings by varying the synthesis parameters (Pierpaoli et al., 2019). The "nano-flaps" are secondary protuberances grown perpendicularly to the surface of the nanowalls due to the absence of a uniform electric field. The density of the "nano-flaps" can be modified *a posteriori* by a capillarity-driven modification process (Bo et al., 2017). The production of uniaxially aligned, controlled porosity may bring the benefits of an effective perpendicular diffusion to the electrode, and minimise the diffusion around it (Ariga et al., 2012). Scanning electron micrographs of the different electrodes, before and after the EO experiment, are reported in Figure 4.

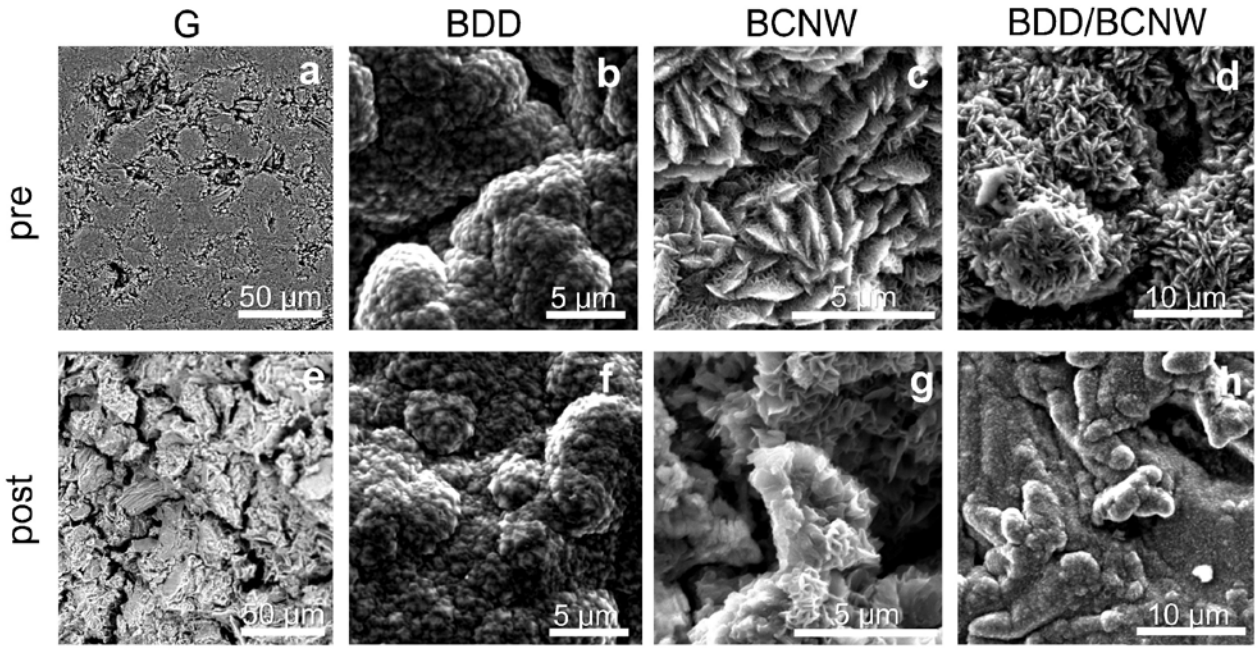

Figure 4 – SEM images of the graphite (G), boron-doped diamond (BDD), boron-doped carbon nanowall (BCNW), and composite (BDD/BCNW) electrodes before (pre) and after (post) the LL EO test.

The graphite electrode (Figure 4a) appears visibly altered after the EO process (Figure 4e), so the test was concluded after 4 h, instead of 8 h. The porosity of the electrode surface significantly increased, as a result of the graphite oxidation and the ion intercalation, present in the leachate. The morphology of the BDD electrode (Figure 4b/f) appears unchanged, while the BCNW electrode (Figure 4c/g) exhibits a partial loss of the thinner nanowalls and the shedding of carbon flakes, partially revealing the Nb substrate. The BDD/BCNW nanoarchitecture, prior the the EO test, exhibits a similar morphology to the BCWN and it visibly change after, tending to look like to the BDD structure, with localized protrusions (Figure 4d/h).

Raman spectroscopy is a relatively simple, quick and non-destructive method to measure the

inelastic light scattering from the sample surface, and is a widely used technique for the characterisation of carbonaceous materials, which can provide useful information on the chemical and molecular morphology. Figure 5 contains the Raman spectra for the four electrodes, before and after the EO test.

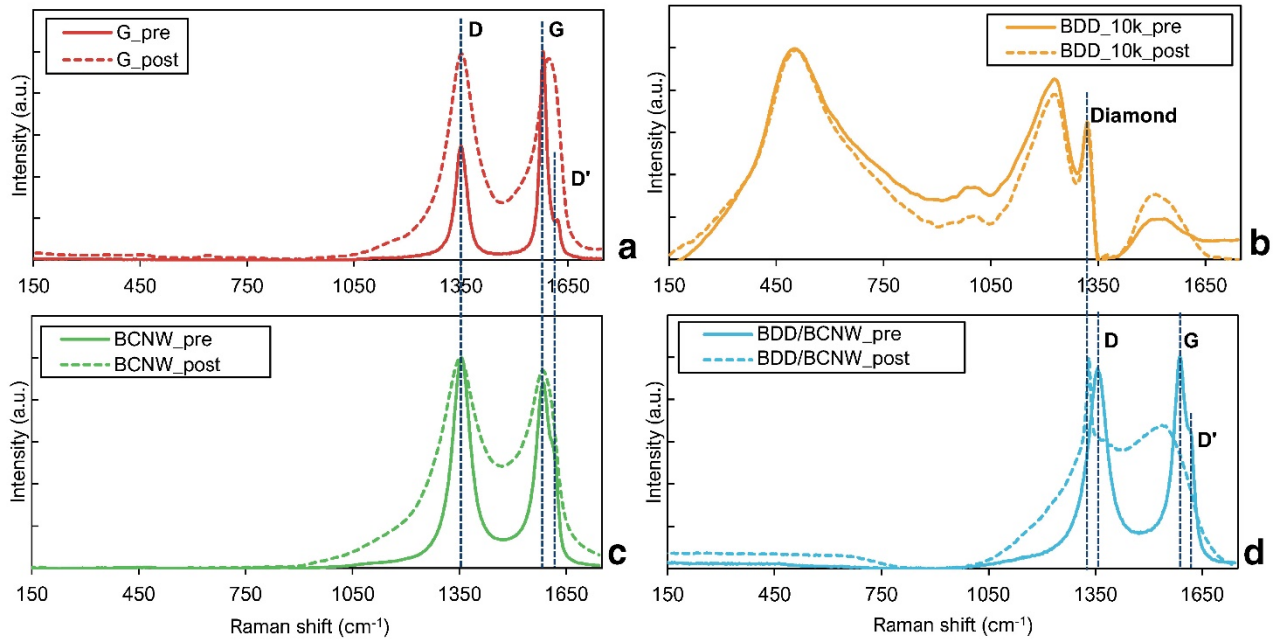

Figure 5 – Raman spectra of the graphite (G), boron-doped diamond (BDD), boron-doped carbon nanowall (BCNW), and composite (BDD/BCNW) electrodes before (pre) and after (post) the LL EO test.

The spectra of the graphite electrode (Figure 5a) report two prominent peaks at about 1353cm^{-1} and 1583 cm^{-1}, corresponding to the G and D bands, respectively, where the D band corresponds to defects or disorders in sp^2 structure especially occurring at the edges of graphene sheets. The G band corresponds to hexagonal carbon rings that arise from in-plane C-C bond stretching vibrations. The broadening and intensity increase of the D band may indicate an increase of disorder after the EO process resulting from oxidation processes and leading to the formation of functional groups, resulting in an increased I_D/I_G ratio (Zhang et al., 2016). The increase of this ratio confirms an increase in defect density in the carbon sp^2 structure (Sahoo and Mallik, 2015). The splitting of the G-band into the D'-band highlights the transformation into a graphitic structure and the formation of defects in the formed sp^2 layers.

In the case of BDD, for both spectra (Figure 5b), it is possible to easily distinguish the diamond peak at 1332 cm^{-1}. The broad band at around 500 cm^{-1} is related to the lesser presence of amorphous carbon, while the additional band at 1520 cm^{-1} was attributed to the C-H bending bonds (Fudala-Ksiazek et al., 2018). As was previously seen in the SEM images, the EO process did not affect the BDD molecular structure. For the BCNW spectra (Figure 5c), two main bands at around 1356 cm^{-1}

and 1590 cm^{-1} are found, generally attributed to the G and D bands. Similarly, for the graphite electrode, the EO process induces a peak widening, due to the increased amount of disorder, even if to a lesser extent due to the almost unaltered I_D/I_G ratio. The pristine BDD/BCNW sample exhibits a spectrum (Figure 5d) similar to that of the BCNW. However, after the EO process, it is possible to observe the appearing of a microcrystalline diamond peak at 1331 cm^{-1}, due to the partial detachment of the overlying BCNW layer. The co-presence of the diamond peak with the D and G bands suggests the mixed presence of sp^2- and sp^3-bonded carbon.

3.3 Electrode electrochemical characterisation

Voltammetric curves are useful for testing the surface quality of electrodes because the electrochemical response is very sensitive to the physicochemical properties of the surface. One of the important parameters describing anodes is their oxygen overpotential. Otherwise, a large amount of delivered electrical energy will be wasted on O_2 production. The nature of the formed oxidants is determined by the electrode's potential window, especially by the one characterised by the high oxygen evolution potential. The anode's oxidation power is directly related to the anode material; the higher O_2 overvoltage, the higher its oxidation power is. Figure 6 shows the resulting cyclic voltammetry curve obtained for the graphite, BDD, BCNW, and BDD/BCNW electrodes.

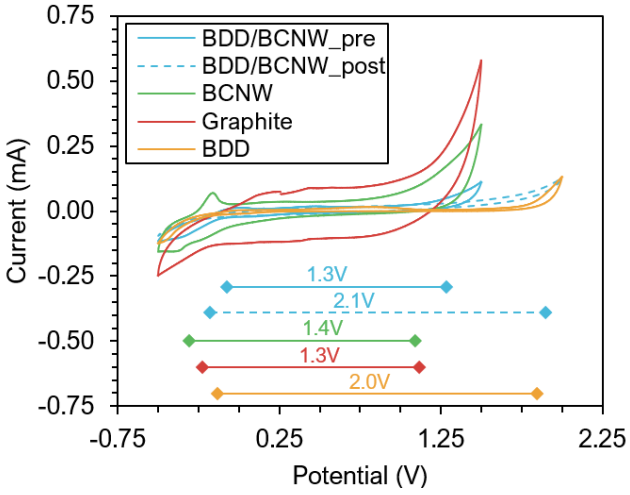

Figure 6 – Cyclic voltammograms of G, BDD, BCNW, and BDD/BCNW electrodes before the EO test. The voltammogram after the EO test has also been reported for the BDD/BCNW electrodes.

BDD is characterised by a very wide electrochemical window. The results showed that the BDD/BCNW electrode, before the oxidation, was electrochemically stable to a potential of about 1.35V which is determined versus an Ag/AgCl electrode. The graphite and BCNW electrodes had a similar oxygen evolution voltage of about 1.2V vs. the Ag/AgCl reference electrode, but the forming double layer capacity was much larger for the graphite electrode, which caused energy loss and a lower current efficiency of the electrochemical oxidation of the leachate. The graphite, BCNW, and BDD/BCNW electrodes had lower oxygen evolution potentials, which produced weaker oxidants

than the anode with a higher oxygen evolution potential (BDD) (Chang et al., 2009). Different anode materials, as well as the type of wastewater, affect the efficiency obtained during electrooxidation. The high overpotential of water decomposition can be an advantage due to the formation of strong oxidants, but it resulted in higher energy consumption during the electrooxidation of pollutants. The electrooxidation mechanism is determined by the formed oxidants as well as the surface adsorption properties, hence the similar BCNW and BDD/BCNW electrooxidation products, and different products for BDD (Martı and Ferro, 2006). After the EO process, the BDD/BCNW composite electrode changed its character tending to a characteristic curve for BDD. High O_2 overvoltage anodes are associated with weaker interaction with the electrode surface and lower ion adsorption (Bergmann et al., 2009; Vatistas, 2012).

Electrochemical impedance spectroscopy (EIS) is a method to characterise the interfacial properties of electrodes (B. Oliveira and Oliveira-Brett, 2010). The impedance measurements were performed in sulphuric acid media at the graphite, BDD, BDD/BCNW, and BCNW electrode surfaces immediately before and after EO of the leachates (Figure 7).

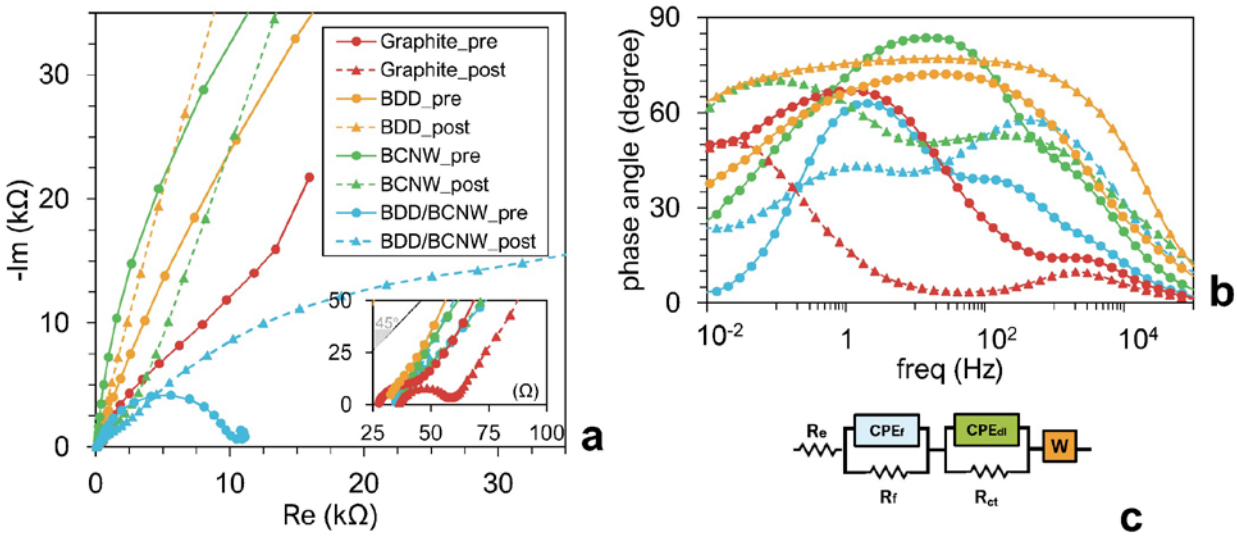

Figure 7 – Impedance spectra of electrodes tested in 0.5m H_2SO_4 as electrolyte vs. Ag/AgCl and electrical equivalent circuit.

The Nyquist spectra (Figure 7a) for the BDD/BCNW prior to the oxidation process had the shape of a flattened semicircle with two visible time constants. For the BDD and BCNW materials before and after the oxidation process, for graphite prior the EO, and for BDD/BCNW after the EO process, the part of the diagrams responsible for diffusion and the semicircle from the charge transfer reactions overlap and create a curved plot line. The curves of Graphite_post, and BDD/BCNW_pre show flattened semicircles and a significant diffusion part for graphite post, while it is inappreciable

at high frequencies for BDD/BCNW_pre.

The two-time constants are visible on the bode curves for the graphite, BDD/BCNW, and BCNW electrodes. Due to the low porosity of BDD, the second time constant is not clearly visible (Figure 7b). The curves shown in Figure 7a were fitted taking into account two-time constants (RC), the reflect film resistance (R_f, CPE_f) and the charge transfer process which took place at the electrode/electrolyte interface (R_{ct}, CPE_{dl}) (Levi and Aurbach, 1997; Siuzdak et al., 2015; Wang et al., 2010). The equivalent electrical circuit (EqEC) is reported in Figure 7c, and the fitted values of the elements in the EqEC are displayed in Table 3.

Table 3 – EIS fitting parameters of the G, BDD, BCNW, and BDD/BCNW electrodes before and after the leachate EO test.

Electrode	R_e	R_{ct}	CPE_{dl}		R_f	CPE_f	
	Ω	Ω	Y_{dl} $Fs^{(\alpha-1)}$	α_{dl}		Y_f $Fs^{(\alpha-1)}$	α_f
Graphite_pre	29.6	$5.1 \cdot 10^{9}$	$1.26 \cdot 10^{-4}$	0.91	$2.69 \cdot 10^{3}$	$5.0 \cdot 10^{-4}$	0.78
Graphite_post	34.8	$2.7 \cdot 10^{3}$	$1.14 \cdot 10^{-2}$	0.72	11.9	$3.7 \cdot 10^{-3}$	0.46
BDD_pre	30.2	$7.3 \cdot 10^{5}$	$1.59 \cdot 10^{-5}$	0.82	$1.1 \cdot 10^{5}$	$1.3 \cdot 10^{-3}$	0.82
BDD_post	10.6	$9.8 \cdot 10^{6}$	$5.19 \cdot 10^{-6}$	0.87	$1.1 \cdot 10^{5}$	$1.5 \cdot 10^{-5}$	0.87
BCNW_pre	33.7	$4.9 \cdot 10^{5}$	$1.52 \cdot 10^{-5}$	0.90	$1.1 \cdot 10^{5}$	$6.2 \cdot 10^{-6}$	0.96
BCNW_post	30.2	$1.9 \cdot 10^{6}$	$1.95 \cdot 10^{-5}$	0.83	$3.6 \cdot 10^{3}$	$2.8 \cdot 10^{-5}$	0.62
BDD/BCNW_pre	33.2	$1.0 \cdot 10^{4}$	$7.59 \cdot 10^{-5}$	0.87	$1.72 \cdot 10^{2}$	$4.8 \cdot 10^{-5}$	0.78
BDD/BCNW_post	31.6	$5.5 \cdot 10^{4}$	$3.82 \cdot 10^{-5}$	0.65	$1.40 \cdot 10^{3}$	$4.0 \cdot 10^{-6}$	0.94

Under perfect conditions, diffusion is represented on a Nyquist plot in the low-frequency part by a 45-degree slope line. For BDD and BCNW before and after the oxidation process, for graphite prior the EO, and for BDD/BCNW post EO, the line (diffusion part) is overlaid with semicircles from charge transfer processes and the film resistance. The recorded spectra (Figure 7a) were analysed using the equivalent electrical circuit consisting of electrolyte resistance (R_{el}) in series with two-time constants (R and C in parallel), including in-place capacitance (C), constant phase element (CPE): R_f, CPE_f and R_{ct}, CPE_{dl} and Warburg element W (Figure 7c). A CPE is generally used when interfacial impedance occurs, and is particularly helpful in describing interface processes on sp^2-based carbon electrodes and other heterogeneous materials.

In contrast to the impedance equation of capacitor C, the expression characterising the impedance (Z) of the CPE contains additional parameter α in the range $0 < \alpha \leq 1$: $Z=Y^{-1}(i\omega)^{-\alpha}$, where ω is the

angular frequency, and Y is the CPE parameter in F $s^{(\alpha-1)}$. The Warburg element is related to the diffusion of charged ions from the bulk of the electrolyte to the surface of the electrode (Ryl et al., 2014; *EC-Lab – Application Note #42*, 2012). The value of the charge transfer resistance, taking into account the electrode surface, evaluated by applying the EqEC was $5.2 \cdot 10^2$ $\Omega \cdot cm^2$ for BDD/BCNW_pre, and was an order of magnitude lower than for BDD_pre ($5.27 \cdot 10^3$ $\Omega \cdot cm^2$) and two orders of magnitude lower than for BCNW_pre (Table 4).

Table 4 – Electrochemical parameters of the equivalent electrical circuit for the prepared electrodes before and after electrochemical oxidation immersed in 0.5 M H_2SO_4

Electrode	$S*R_{ct}$ $cm^2 \cdot \Omega$	j_0EIS $A \cdot cm^{-2}$	j_0Tafel $A \cdot cm^{-2}$
Graphite_pre	$2.95 \cdot 10^5$	$8.86 \cdot 10^{-8}$	$7.38 \cdot 10^{-6}$
Graphite_post	$1.35 \cdot 10^2$	$1.95 \cdot 10^{-4}$	$4.40 \cdot 10^{-4}$
BDD-10k_pre	$5.27 \cdot 10^3$	$4.96 \cdot 10^{-6}$	$5.00 \cdot 10^{-7}$
BDD-10_post	$5.34 \cdot 10^3$	$4.90 \cdot 10^{-6}$	$6.20 \cdot 10^{-7}$
BCNW_pre	$2.45 \cdot 10^4$	$1.07 \cdot 10^{-6}$	$1.50 \cdot 10^{-6}$
BCNW_post	$9.52 \cdot 10^4$	$2.75 \cdot 10^{-7}$	$3.80 \cdot 10^{-7}$
BDD/BCNW_pre	$5.20 \cdot 10^2$	$5.03 \cdot 10^{-5}$	$2.86 \cdot 10^{-6}$
BDD/BCNW_post	$2.74 \cdot 10^3$	$9.54 \cdot 10^{-6}$	$1.06 \cdot 10^{-5}$

Charge transfer resistances may be converted into exchange current densities (j_0) by the following equation:

$$j_0 = \frac{RT}{F}\frac{1}{SR_{ct}}$$

where R is the gas constant, F is the Faraday constant, and SR_{ct} leads the resistance of the real electrode surface.

The exchange current density shown in Table 4 is on the order of 10^{-8} $A \cdot cm^{-2}$ ($8.86 \cdot 10^{-8}$ $A \cdot cm^{-2}$) for the graphite, prior to the EO test, and about four orders of magnitude higher for the graphite after the EO test ($1.95 \cdot 10^{-4}$ $A \cdot cm^{-2}$). This behaviour is caused by the increase of the surface area by graphite exfoliation (Zhang et al., 2016) during oxidation of organic compounds on the graphite electrode.

For the BCNW and BDD/BCNW electrodes, a decrease in the exchange current density for the electrodes after the EO process by one order of magnitude was observed, according to the R_{ct} values obtained from EIS. For the BDD electrodes, the exchange current density remained unchanged after

411 the electrooxidation process. This indicates the stability of the BDD electrodes. However, it should
412 be noted that the largest exchange current density is was revealed by the BDD/BCNW electrodes,
413 which relates to the larger active surface area of the resulting BDD/BCNW electrodes than the
414 electrodes grown directly on the niobium surface. The BCNW electrodes had the same order of
415 magnitude of exchange current density as the BDD electrodes. After the oxidation process, the
416 exchange current density of the BDD/BCNW electrode decreased to a value equivalent to the
417 exchange current density of the BDD electrodes. This suggests degradation of the BCNW layer on
418 the BDD electrode with mainly the BDD layer remaining.

419 The exchange current density values were low and indicate that the charge transfer process may be
420 a stage limiting the EO process. Therefore, the BDD/BCNW_pre exchange current was greater by
421 one order of magnitude than for BDD_pre, and BCNW_pre indicates a good direction of
422 modification of electrodes, and shows that the charge transfer process prefers BDD/BCNW as the
423 electrode for the electrochemical oxidation reaction. A lower charge transfer resistance means a
424 higher exchange current and thus a faster electrochemical oxidation process. It should be
425 emphasised that an increase in the current density does not necessarily lead to an increase in the
426 oxidation efficiency or oxidation rate. For a given anode material, the impact of current density on
427 the electrooxidation efficiency of treated wastewater depends on their physicochemical properties
428 such as the type and concentration of the electrolyte, pH value, and temperature (Anglada et al.,
429 2009). However, the adhesion to the substrate of the material being produced will need to be
430 improved so that it does not degrade during electrooxidation.

431 The exchange current density can be estimated using also the Tafel extrapolation method and a
432 transformation of the Butler-Volmer equation. It should be taken into account that the error of this
433 method increases in the presence of adsorbed or passive layers. In these cases, thanks to the use of
434 EIS, we can afford to evaluate the kinetics of the oxidation process on electrodes. Table 4 reports the
435 comparison of the exchange current density estimated with the two methods. It can be seen that the
436 exchange current density obtained from the Tafel plots differs from the exchange current density
437 estimated by the EIS method for most electrodes. The obtained values of exchange current are only
438 of the same order for the BCNW electrodes.

439 ## 4. Conclusions

440 Architecturing carbon nanostructures represents valuable support to enhance the
441 electrochemical properties of anodes for environmental remediation. Because of the lower surface
442 resistance, higher surface area and current exchange density, the fabricated nanostructured
443 electrodes exhibit an increased process efficiency.

444 The localised pH variation within the BCNW nanostructure may be responsible for the limited

competition between the direct oxidation of organics and other secondary undesired electrochemical reactions initiated by chlorate intermediates. This aspect results in enhanced COD (and BOD) removal by the composite nanostructure, compared to BDD, at the expense of $N\text{-}NH_4^+$ mineralisation, which is mediated mainly by secondary reactions, despite both electrodes working at the same potential.

The potential of oxygen evolution revealed by cyclic voltammetry was similar for graphite, BCNW, and BDD/BCNW, and higher for BDD. The maze-like structure of the BCNW significantly increased the active sites, improving the exchange current density. After the EO test, the morphology and electrochemical character of the BDD/BCNW architecture changed, exhibiting a coexistence of sp^2 and sp^3 carbon. While a higher sp^2/sp^3 ratio is generally used as a descriptor of the BDD quality, which negatively affects the mineralisation efficiency, the localised sp^2 inhomogeneity left by the etched BCNW may be the reason for the improved efficiency.

Acknowledgements

This research was supported by the Polish National Agency for Academic Exchange (NAWA), under the Ulam program, Agreement no. PPN/ULM/2019/1/00061/DEC/1 (M.Pierpaoli).

This work was also supported by the Provincial Fund for Environmental Protection and Water management in Gdansk under Grant No. RX15/13/2017.

Bibliography

Anglada, A., Urtiaga, A., Ortiz, I., 2009. Contributions of electrochemical oxidation to waste-water treatment: fundamentals and review of applications. J. Chem. Technol. Biotechnol. 84, 1747–1755. https://doi.org/10.1002/jctb.2214

Ariga, K., Vinu, A., Yamauchi, Y., Ji, Q., Hill, J.P., 2012. Nanoarchitectonics for Mesoporous Materials. Bull. Chem. Soc. Jpn. 85, 1–32. https://doi.org/10.1246/bcsj.20110162

B. Oliveira, S.C., Oliveira-Brett, A.M., 2010. Voltammetric and electrochemical impedance spectroscopy characterization of a cathodic and anodic pre-treated boron doped diamond electrode. Electrochim. Acta 55, 4599–4605. https://doi.org/10.1016/j.electacta.2010.03.016

Bashir, M.J.K., Isa, M.H., Kutty, S.R.M., Awang, Z. Bin, Aziz, H.A., Mohajeri, S., Farooqi, I.H., 2009. Landfill leachate treatment by electrochemical oxidation. Waste Manag. 29, 2534–2541. https://doi.org/10.1016/J.WASMAN.2009.05.004

Bergmann, M.E.H., Rollin, J., Iourtchouk, T., 2009. The occurrence of perchlorate during drinking water electrolysis using BDD anodes. Electrochim. Acta 54, 2102–2107. https://doi.org/10.1016/j.electacta.2008.09.040

Bo, Z., Tian, Y., Han, Z.J., Wu, S., Zhang, S., Yan, J., Cen, K., Ostrikov, K., 2017. Tuneable fluidics within graphene nanogaps for water purification and energy storage. Nanoscale Horizons 2,

89–98. https://doi.org/10.1039/c6nh00167j

Bogdanowicz, R., Fabiańska, A., Golunski, L., Sobaszek, M., Gnyba, M., Ryl, J., Darowicki, K., Ossowski, T., Janssens, S.D., Haenen, K., Siedlecka, E.M., 2013. Influence of the boron doping level on the electrochemical oxidation of the azo dyes at Si/BDD thin film electrodes. Diam. Relat. Mater. 39, 82–88. https://doi.org/10.1016/J.DIAMOND.2013.08.004

Chang, M., Gao, C., Jiang, J., 2009. Electrochemical oxidation of organic compounds using boron-doped diamond electrode. J. Electrochem. Soc. 156, 50–54. https://doi.org/10.1149/1.3042220

Chiang, L.-C., Chang, J.-E., Wen, T.-C., 1995. Indirect oxidation effect in electrochemical oxidation treatment of landfill leachate. Water Res. 29, 671–678. https://doi.org/10.1016/0043-1354(94)00146-X

D. Eaton, A., H. Franson, M.A., American Public Health Association (Eds.), 2005. Standard Methods for the Examination of Water & Wastewater, 21st ed. Amer Public Health Assn.

Dettlaff, A., Jakóbczyk, P., Ficek, M., Wilk, B., Szala, M., Wojtas, J., Ossowski, T., Bogdanowicz, R., 2020. Electrochemical determination of nitroaromatic explosives at boron-doped diamond/graphene nanowall electrodes: 2,4,6-trinitrotoluene and 2,4,6-trinitroanisole in liquid effluents. J. Hazard. Mater. 387, 121672. https://doi.org/10.1016/j.jhazmat.2019.121672

Dutta, S., Bhaumik, A., Wu, K.C.W., 2014. Hierarchically porous carbon derived from polymers and biomass: Effect of interconnected pores on energy applications. Energy Environ. Sci. 7, 3574–3592. https://doi.org/10.1039/c4ee01075b

Dutta, S., Kim, J., Ide, Y., Ho Kim, J., Hossain, M.S.A., Bando, Y., Yamauchi, Y., Wu, K.C.W., 2017. 3D network of cellulose-based energy storage devices and related emerging applications. Mater. Horizons. https://doi.org/10.1039/c6mh00500d

European Parliament, 2013. Directive 2013/39/EU of the European Parliament and of the Council of 12 August 2013 amending Directives 2000/60/EC and 2008/105/EC as regards priority substances in the field of water policy Text with EEA relevance.

European Parliament, n.d. Council Directive 1999/31/EC of 26 April 1999 on the landfill of waste. Off. J. L 182 , 16/07/1999 P. 0001 - 0019.

Fudala-Ksiazek, S., Pierpaoli, M., Kulbat, E., Luczkiewicz, A., 2016. A modern solid waste management strategy - the generation of new by-products. Waste Manag. 49, 516–529. https://doi.org/10.1016/j.wasman.2016.01.022

Fudala-Ksiazek, S., Pierpaoli, M., Luczkiewicz, A., 2017. Fate and significance of phthalates and bisphenol A in liquid by-products generated during municipal solid waste mechanical-biological pre-treatment and disposal. Waste Manag. 64, 28–38. https://doi.org/10.1016/j.wasman.2017.03.040

Fudala-Ksiazek, S., Sobaszek, M., Luczkiewicz, A., Pieczynska, A., Ofiarska, A., Fiszka-Borzyszkowska, A., Sawczak, M., Ficek, M., Bogdanowicz, R., Siedlecka, E.M., 2018. Influence of the boron doping level on the electrochemical oxidation of raw landfill leachates: Advanced pre-treatment prior to the biological nitrogen removal. Chem. Eng. J. 334, 1074–1084. https://doi.org/10.1016/j.cej.2017.09.196

Hiramatsu, M., Hori, M., 2010. Carbon Nanowalls: Synthesis and Emerging Applications.

Huang, H., Yan, M., Yang, C., He, H., Jiang, Q., Yang, L., Lu, Z., Sun, Z., Xu, X., Bando, Y., Yamauchi, Y., 2019. Graphene Nanoarchitectonics: Recent Advances in Graphene-Based Electrocatalysts for Hydrogen Evolution Reaction. Adv. Mater. 31, 1903415. https://doi.org/10.1002/adma.201903415

Kaneti, Y.V., Dutta, S., Hossain, M.S.A., Shiddiky, M.J.A., Tung, K.L., Shieh, F.K., Tsung, C.K., Wu, K.C.W., Yamauchi, Y., 2017. Strategies for Improving the Functionality of Zeolitic Imidazolate Frameworks: Tailoring Nanoarchitectures for Functional Applications. Adv. Mater. 29. https://doi.org/10.1002/adma.201700213

Levi, M.D., Aurbach, D., 1997. Simultaneous measurements and modeling of the electrochemical impedance and the cyclic voltammetric characteristics of graphite electrodes doped with lithium. J. Phys. Chem. B 101, 4630–4640. https://doi.org/10.1021/jp9701909

Malgras, V., Ji, Q., Kamachi, Y., Mori, T., Shieh, F.K., Wu, K.C.W., Ariga, K., Yamauchi, Y., 2015. Templated synthesis for nanoarchitectured porous materials. Bull. Chem. Soc. Jpn. 88, 1171–1200. https://doi.org/10.1246/bcsj.20150143

Martı, C.A., Ferro, S., 2006. Electrochemical oxidation of organic pollutants for the wastewater treatment□: direct and indirect processes 1324–1340. https://doi.org/10.1039/b517632h

Medeiros De Araújo, D., Cañizares, P., Martínez-Huitle, C.A., Rodrigo, M.A., 2014. Electrochemical conversion/combustion of a model organic pollutant on BDD anode: Role of sp3/sp2 ratio. Electrochem. commun. 47, 37–40. https://doi.org/10.1016/j.elecom.2014.07.017

Pelaez, A.I., Sanchez, J., Almendros, G., 2009. Bioreactor treatment of municipal solid waste landfill leachates: Characterization of organic fractions. Waste Manag. 29, 70–77. https://doi.org/10.1016/j.wasman.2008.05.003

Pierpaoli, M., Ficek, M., Rycewicz, M., Sawczak, M., Karczewski, J., Ruello, M., Bogdanowicz, R., 2019. Tailoring Electro/Optical Properties of Transparent Boron-Doped Carbon Nanowalls Grown on Quartz. Materials (Basel). 12, 547. https://doi.org/10.3390/ma12030547

Pierpaoli, M., Lewkowicz, A., Rycewicz, M., Szczodrowski, K., Ruello, M.L., Bogdanowicz, R., 2020a. Enhanced photocatalytic activity of transparent carbon nanowall/TiO_2 heterostructures. Mater. Lett. 262. https://doi.org/10.1016/j.matlet.2019.127155

Pierpaoli, M., Rycewicz, M., Łuczkiewicz, A., Fudala-Książek, S., Bogdanowicz, R., Ruello, M.L., 2020b. Electrodes criticality: the impact of CRMs in the leachate electrochemical oxidation. Manuf. Rev. 7, 7. https://doi.org/10.1051/MFREVIEW/2020006

Qiao, M.X., Zhang, Y., Zhai, L.F., Sun, M., 2018. Corrosion of graphite electrode in electrochemical advanced oxidation processes: Degradation protocol and environmental implication. Chem. Eng. J. 344, 410–418. https://doi.org/10.1016/j.cej.2018.03.105

Ryl, J., Bogdanowicz, R., Slepski, P., Sobaszek, M., Darowicki, K., 2014. Dynamic electrochemical impedance spectroscopy (deis) as a tool for analyzing surface oxidation processes on boron-doped diamond electrodes. J. Electrochem. Soc. 161, 0–7. https://doi.org/10.1149/2.016406jes

Sahoo, S.K., Mallik, A., 2015. Simple, fast and cost-effective electrochemical synthesis of few layer graphene nanosheets. Nano 10, 1–10. https://doi.org/10.1142/S1793292015500198

Sirés, I., Brillas, E., Oturan, M.A., Rodrigo, M.A., Panizza, M., 2014. Electrochemical advanced oxidation processes: Today and tomorrow. A review. Environ. Sci. Pollut. Res. 21, 8336–8367. https://doi.org/10.1007/s11356-014-2783-1

Siuzdak, K., Bogdanowicz, R., Sawczak, M., Sobaszek, M., 2015. Enhanced capacitance of composite TiO_2 nanotube/boron-doped diamond electrodes studied by impedance spectroscopy. Nanoscale 7, 551–558. https://doi.org/10.1039/c4nr04417g

Sobaszek, M., Siuzdak, K., Ryl, J., Sawczak, M., Gupta, S., Carrizosa, S.B., Ficek, M., Dec, B., Darowicki, K., Bogdanowicz, R., 2017. Diamond Phase (sp^3-C) Rich Boron-Doped Carbon Nanowalls (sp^2-C): Physicochemical and Electrochemical Properties. J. Phys. Chem. C 121, 20821–20833. https://doi.org/10.1021/acs.jpcc.7b06365

573 Spagni, A., Marsili-Libelli, S., Lavagnolo, M.C., 2008. Optimisation of sanitary landfill leachate
574 treatment in a sequencing batch reactor. Water Sci. Technol. 58, 337–343.
575 https://doi.org/10.2166/wst.2008.399

576 Tan, C., Xiang, B., Li, Y., Fang, J., Huang, M., 2011. Preparation and characteristics of a nano-PbO_2
577 anode for organic wastewater treatment. Chem. Eng. J. 166, 15–21.
578 https://doi.org/10.1016/j.cej.2010.08.018

579 The modified inductance element La, EC-Lab – Application Note #42 08/2012, 2012. . 4 Rue de
580 Vaucanson, 38170 Seyssinet-Pariset, FRANCE.

581 Vatistas, N., 2012. Electrocatalytic Properties of BDD Anodes: Its Loosely Adsorbed Hydroxyl
582 Radicals. Int. J. Electrochem. 2012, 1–7. https://doi.org/10.1155/2012/507516

583 Wang, D., Ye, Q., Yu, B., Zhou, F., 2010. Towards chemically bonded p-n heterojunctions through
584 surface initiated electrodeposition of p-type conducting polymer inside TiO2 nanotubes. J.
585 Mater. Chem. 20, 6910–6915. https://doi.org/10.1039/c0jm00743a

586 Wang, J., Xu, Y., Ding, B., Chang, Z., Zhang, X., Yamauchi, Y., Wu, K.C.-W., 2018. Confined Self-
587 Assembly in Two-Dimensional Interlayer Space: Monolayered Mesoporous Carbon
588 Nanosheets with In-Plane Orderly Arranged Mesopores and a Highly Graphitized Framework.
589 Angew. Chemie Int. Ed. 57, 2894–2898. https://doi.org/10.1002/anie.201712959

590 Wang, Q., Jin, T., Hu, Z., Zhou, L., Zhou, M., 2013. TiO_2-NTs/SnO_2-Sb anode for efficient
591 electrocatalytic degradation of organic pollutants: Effect of TiO2-NTs architecture AADRT.
592 Sep. Purif. Technol. 102, 180–186. https://doi.org/10.1016/j.seppur.2012.10.006

593 Zhang, G., Wen, M., Wang, S., Chen, J., Wang, J., 2016. Insights into electrochemical behavior and
594 anodic oxidation processing of graphite matrix in aqueous solutions of sodium nitrate. J. Appl.
595 Electrochem. 46, 1163–1176. https://doi.org/10.1007/s10800-016-0999-0

596 Zhang, L., Xu, L., He, J., Zhang, J., 2014. Preparation of Ti/SnO_2-Sb electrodes modified by carbon
597 nanotube for anodic oxidation of dye wastewater and combination with nanofiltration.
598 Electrochim. Acta 117, 192–201. https://doi.org/10.1016/j.electacta.2013.11.117

599